SIMULATION OF FULL-WAVEFORM LASER ALTIMETER ECHO WAVEFORM

Y. Lv, X.H. Tong, S.J. Liu, H. Xie, K.F. Luan, J. Liu

College of Surveying and Geo-Informatics, Tongji University, 1239 Siping Road, Shanghai, 200092, China
dqsy2006@126.com

Commission I, WG I/2

KEY WORDS: Full-waveform, Altimeter, Simulation, Effect factor, Different terrains

ABSTRACT:

Change of globe surface height is an important factor to study human living environment. The Geoscience Laser Altimeter System (GLAS) on ICESat is the first laser-ranging instrument for continuous global observations of the Earth. In order to have a comprehensive understanding of full-waveform laser altimeter, this study simulated the operating mode of ICESat and modeled different terrains' (platform terrain, slope terrain, and artificial terrain) echo waveforms based on the radar equation. By changing the characteristics of the system and the targets, numerical echo waveforms can be achieved. Hereafter, we mainly discussed the factors affecting the amplitude and size (width) of the echoes. The experimental results implied that the slope of the terrain, backscattering coefficient and reflectivity, target height, target position in the footprint and area reacted with the pulse all can affect the energy distribution of the echo waveform and the receiving time. Finally, Gaussian decomposition is utilized to decompose the echo waveform. From the experiment, it can be noted that the factors which can affect the echo waveform and by this way we can know more about large footprint full-waveform satellite laser altimeter.

1. INTRODUCTION

Nowadays, laser altimeters placed on different platforms (airborne, satellite) have been widely used in lots of areas like mass balance estimation in Antarctica, vegetation vertical structure, long trend monitor of sea level and so on (Anderson et al., 2005; Alexander et al., 2010; Garvin et al., 1998; Gong et al., 2011; Hyyppä et al., 2001; Joerg, et al., 2015; Means and Acker, 1999; Næsset and Bjerknes, 2001; Nilsson, 1996; Smith et al., 1998; Tian et al.,2015). For the reason that the measurement of altimeter can not only provide high precision elevation or distance information, it can also record the complete waveform of the backscattered signal echo, especially for the full-waveform laser altimeter (Mallet, 2009). A good example is the instrument Geoscience Laser Altimeter System (GLAS) placed on the Ice, Cloud and Land Elevation Satellite (ICESat) launched by NASA in 2003.

The GLAS on the ICESat has two laser channels: 1064nm for surface altimetry and dense clouds, 532nm for the vertical distribution of clouds and aerosols (Wang et al., 2011; Zwally et al., 2002). The fundamental parameters of ICESat are described in Table 1. The GLAS instrument records the signal from the entire time-of-flight of the 1064nm pulse to range from the spacecraft to the target. And by analysing the echo waveform, geophysical parameters will be obtained from waveform.

GLAS Parameters	Value
Emitted pulse energy	75mj (1064nm)
FWHM	4ns
Orbit altitude	598km
Incidence angle	< 5 °
The antenna aperture	100cm

Table 1. Fundamental parameters of ICESat

This paper mainly focuses on the factors affecting the echo waveform, especially for the width and amplitude of the waveform, based on simulation of different terrain surfaces and transmitted pulse parameters.

2. THEORETICAL BASIS

Since the instrument emits the pulse, the pulse transmits through the air and reacts with the targets, then reflects back to the instrument through the air. Altimeter records the round-trip time to measure the target's height. In addition, since the instrument is quite far away from the earth surface, the illuminated footprint is very large. In this article, the emitted pulse is simulated as a Gaussian waveform.

The theoretical basis is the radar equation (Equation (1) and Equation (2)), more details are described in (Abshire et al., 2005; Wagner et al., 2006).

$$P_{R,i}(t)=\sum_{i=1}^{N}\varepsilon_i\frac{4P_T(t)}{\pi R^2\beta_t^2}\rho_i A_{s,i}\frac{1}{\Omega_i R^2}\cdot\frac{\pi D_r^2}{4}\eta_{sys}\eta_{atm} \quad (1)$$

$$\varepsilon_i=\frac{2}{\pi ab}\cdot\exp\left\{-\frac{1}{2}\left[\left(\frac{2x_i}{a}\right)^2+\left(\frac{2y_i}{b}\right)^2\right]\right\}\cdot\frac{\pi R_0^2\beta_t^2}{4} \quad (2)$$

Where, i is the serial number of targets; N is total number of targets; $P_{R,i}(t)$ is the energy of target i echo waveform at time t ; $P_T(t)$ is the energy of the emitted pulse at time t ; β_t is beam width of transmitted pulse; ρ_i is the reflectivity of target i ; $A_{s,i}$ is the area irradiated by the pulse energy; R_i is the distance between target i and transmitter; Ω_i is the backscattering angle of the target; D_R is the diameter of the receiving antenna aperture; η_{atm} is the atmospheric influence to signal; η_{sys} is the systemic influence to signal; a and b is the footprint elliptical semi-major axis and semi-minor axis,

respectively; x_i and y_i is perpendicular distance from target i to semi-major axis and semi-minor axis, respectively.

From the radar equation, we can see that it can be separated into two parts: the instrument factors and the target factors (in this article, we ignore the atmosphere and system effects and set η_{atm} and η_{sys} as constant 1).

Usually, the echo waveform can be seen as a replica of the transmitted pulse (Słota, 2015). The transmitted pulse is described in Equation (3) and Equation (4).

$$P_T(t) = A_T \exp\left\{-\frac{(t-t_{C,T})^2}{2s_T^2}\right\} \quad (3)$$

$$S_T = \frac{FWHM}{2\sqrt{2\ln 2}} \quad (4)$$

Where, A_T is the emitted energy; $t_{C,T}$ is the position of the peak; Full width at half maximum (FWHM) is the term commonly used to describe the size of a pulse, rather than standard deviation s_T .

3. SIMULATION OF THE TARGET ECHO WAVEFORM

There are a variety of terrains on the earth like flat terrain, slope terrain, artificial building terrain and so on. The emitted pulse can be seen as an elliptical or round Gaussian wave when reaches the earth surface after beam spreading.

In order to simulate the Gaussian echo waveform, we set a local cartesian coordinate system, regarding the footprint center as the origin of coordinates and treating the semi-major axis and semi-minor axis of the ellipse as the horizontal and vertical axis. In the footprint, the energy is not evenly distributed. The footprint is separated into several same size bins about 0.1m*0.1m (Figure 1). Finally, the total energy of these bins is regarded as the echo energy.

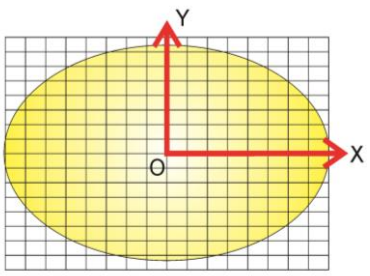

Figure 1. Footprint divided into several same bins.

For the flat terrain, if the Gaussian wave is emitted perpendicular down to the earth, the footprint can be seen as round. If the emitted pulse has an emission angle, the echo waveform is similar to a slope terrain.

For the case of slope terrain, the footprint is ellipse. And the echo waveform will be extended to a wider one, because the bins along the semi-major axis direction in the footprint have different height.

As for the artificial building terrain, the buildings are divided into different height levels and the sum of different levels energy is considered to be the echo energy.

Once the terrain model is simulated, the echo waveform can be obtained. And the echo waveform is treated as the combination of several targets' Gaussian echo waves. So Gaussian decomposition (Brenner et al., 2003) is done to each echo waveform and the parameters of the waveform like amplitude and size (FWHM) are achieved.

4. RESULTS AND DISCUSSION

4.1 The flat terrain

The pulse transmits from the instrument to the target, in this course, the pulse is considered to propagate in a cone. Hereafter, the pulse reacts with the targets, and each target has its unique reflectivity and backward scattering coefficient.

For the flat terrain, we changed the reflectivity and backscattering coefficient, respectively. We simulated echo waveforms of different cases. In this part we mainly discussed the change of the echo waveform amplitude and width. From Figure 2, we can find that the echo energy became lower when the reflectivity turned lower. But the width of the echo waveform was not change.

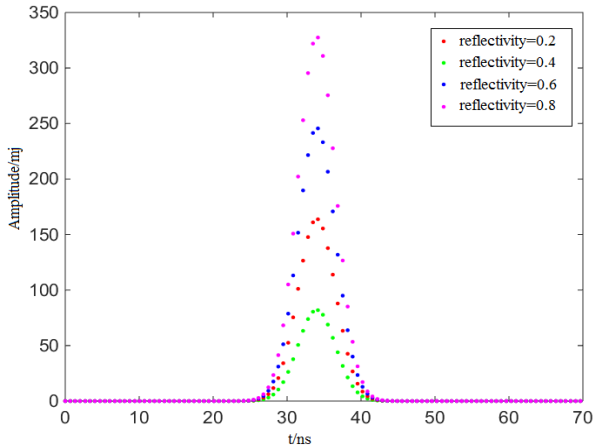

Figure 2. Echo waveforms with different reflectivity.

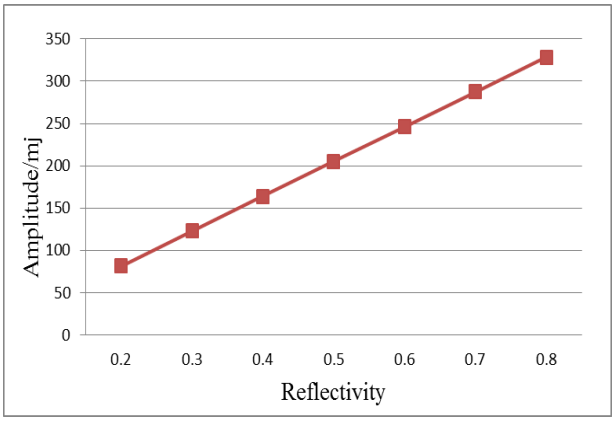

Figure 3. Amplitude of different reflectivity

Figure 3 showed the echo amplitudes when reflectivity changed

from 0.2 to 0.8. The change of amplitude was positively correlated with the reflectivity change.
While changing the backscatter coefficient as 50urad, 100urad, 200urad, 300urad and 350urad, the echoes were shown in Figure 4. It can be obviously noted that if the backscattering angle turned bigger, the received energy became lower In Figure 5, it showed the results of the change of amplitudes with different reflectivity ρ and backscattering angles.

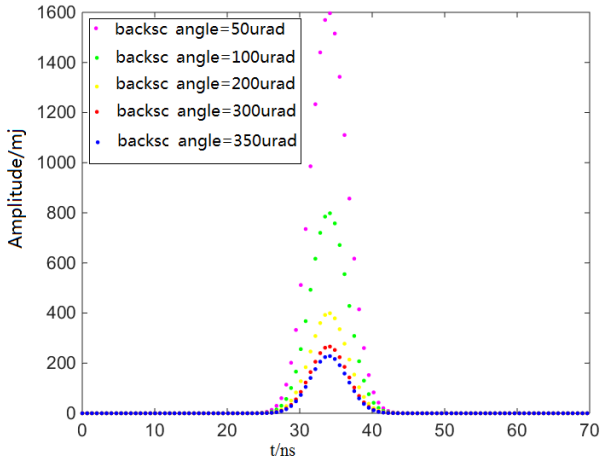

Figure 4. Echo waveforms with different backscattering angles

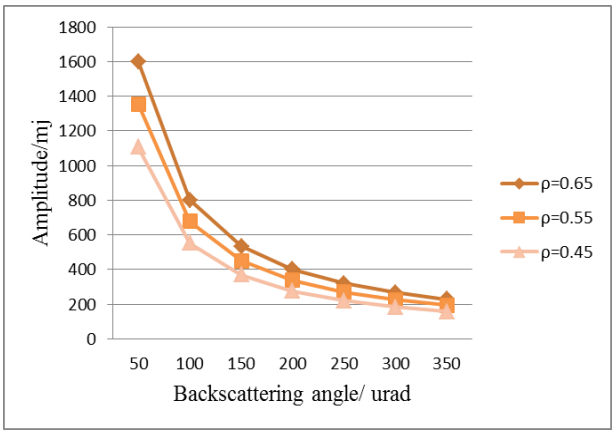

Figure 5. Amplitudes of different reflectivity and backscattering angles

4.2 The slope terrain

Because the earth surface is not always flat, it includes lots of terrains with slope, e.g. mountain, hills and dunes. It is very necessary to analyse the effect of slope to the echo waveforms.

We simulated various slope angles to the terrain. Figure 6 demonstrated that the amplitude became lower if the angle turned bigger, and the size (width) became wider. Also, the start time and end time of the recorded echo is changed with different slope angles. To know more about the relationship between echo waveform and terrain slope, the echoes with different emitted pulse sizes were compared. The results were presented in Figure 7 and Figure 8.

Figure 7 mainly described the change of echo amplitude. It can be seen that, the echo energy with various emitted pulse sizes all became lower as the slope angle turned bigger. They almost had the similar trend. However, the wider emitted pulse size, the smaller energy declining rate with the increase of slope angle.

Figure 8 illustrated the echo size change with different conditions. The echo size became wider while increasing the slope angle, but the echo size was less affected by the emitted pulse size.

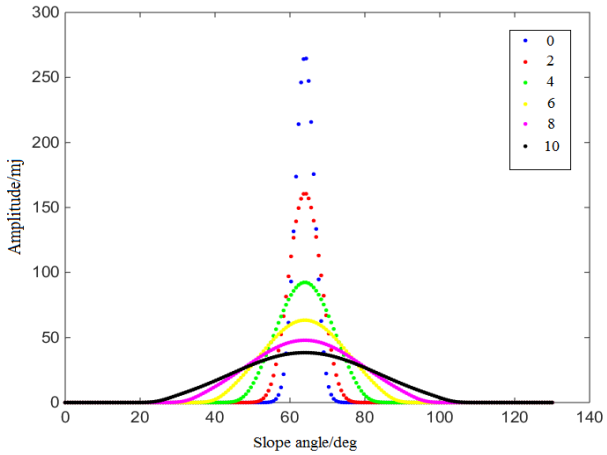

Figure 6. The echo waveform of different slope angles

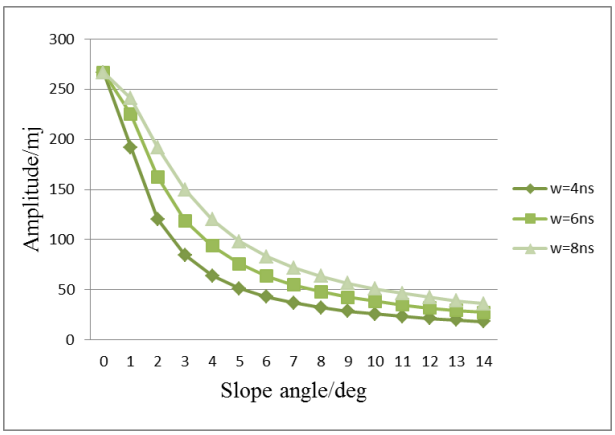

Figure 7. The change of amplitude in different conditions

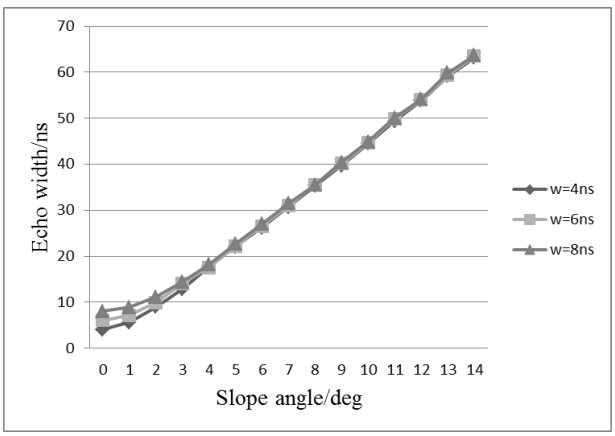

Figure 8. The change of waveform size in different conditions

4.3 The artificial terrain

For artificial terrain, the most common targets are buildings

with different height. Location in the footprint, area of the building roof reacted with pulse and building height are the three main aspects considered in this article.

First, we set different height to one building in the footprint, assuming that the building located half of the footprint. From Figure 9, it could be found that the building amplitude (the first peak) was not changed. However, as the building height increased, the building echo wave was farther from the surface echo wave and the receiving time is more front. The distance between the earth surface and the transmitter was constant, so the last peak (the echo wave of the earth) in the full-waveform was not moved.

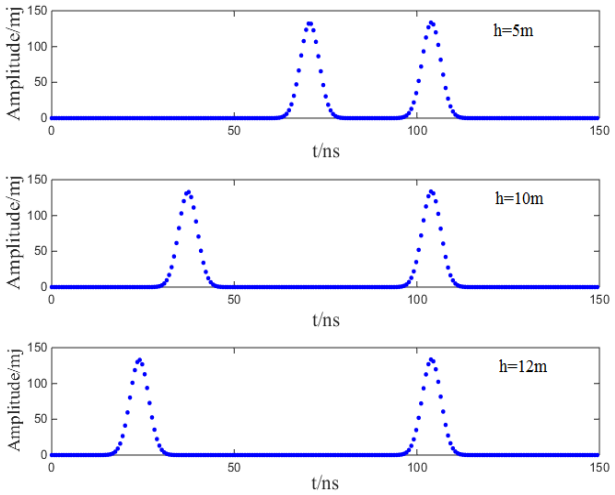

Figure 9. Echo waveform of different height building

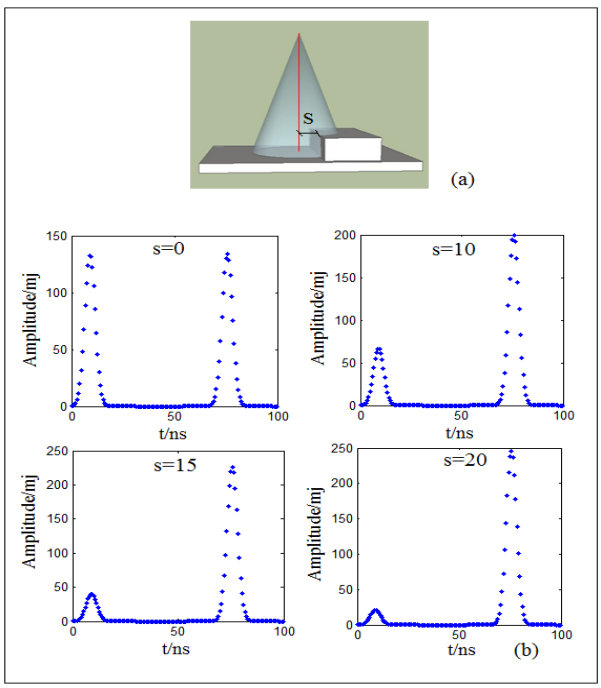

Figure 10. (a) Sketch map of the relative position between footprint and building; (b) The echoes of different building locations.

Secondly, we made different building locations. The distance *s* from the building edge to the footprint center was changed (Figure 10 (a)), in this case, the building was assumed to be larger than the footprint. Figure 10 (b) showed that the closer the distance from building edge to the footprint center, the larger building amplitude was. This meant the building received more energy. The position of the building echo waveform was not move, because the height of the building was still.

5. CONCLUSIONS

In this article, we analysed the factors affecting the echo waveform of full-waveform altimeter comprehensively. Three terrains (flat terrain, slope terrain, artificial terrain) were mainly discussed. We found that the amplitude of the echo was not only relative to the emitted pulse energy, it also related to the terrain's physical characteristics: reflectivity and backscattering coefficient. In addition, the terrain slope angle can affected the amplitude significantly. For the size of the echo, the effective factors included terrain slope angle and emitted pulse size. As for the receiving time of the echo, both of target height and terrain slope had strong impact on it.

Through the experiments in this paper, we knew the echo waveform with a deep understanding. The results will help us to deal with the real data more accurately in a complicated environment, and it even contributes to design the parameters of the altimeter instrument.

REFERENCES

Alexander, C., Tansey, K., Kaduk, J., Holland, D., Tate, N.J., 2010. Backscatter coefficient as an attribute for the classification of full-waveform airborne laser scanning data in urban areas. *ISPRS Journal of Photogrammetry and Remote Sensing*, 65, pp. 423-432.

Anderson, H.E., McGaughey, R.J., Reutebuch, S.E., 2005. Estimating forest canopy fuel parameters using LIDAR data. *Remote Sensing of Environment*, 94(4), pp. 441-449.

Abshire, J., Sun, X., Riris, H., Sirota, M., McGarry, J., Palm, S., Yi, D., Liiva, P., 2005. Geoscience laser altimeter system (glas) on the icesat mission:On-orbit measurement performance. *Geophysical Research Letters*, 32, pp. L21S02.

Brenner, A.C., Zwally, H.J., Bentley, C.R., Csathó, B.M., Harding, D.J., Hofton, M.A., Minster, J.B., Roberts, L., Saba, J.L., Thomas, R.H., Yi, D., 2003. Derivation of range and range distributions from laser pulse waveform analysis for surface elevations, roughness, slope, and vegetation heights.

Garvin, J.B., Bufton, J., Blair, J., Harding, D., Luthcke, S., Frawley, J., Rowlands, D., 1998. Observations of the Earth's topography from the Shuttle Laser Altimeter (SLA): Laser-pulse Echo-recovery measurements of terrestrial surfaces. *Physics and Chemistry of the Earth*, 23, pp. 1053-1068.

Gong, P, Li, Z., Huang, H., Sun, G., Wang, L., 2011. ICESat GLAS data for urban environment monitoring. *IEEE Transactions on Geoscience and Remote Sensing*, 49(3), pp. 1158-1172.

Hyyppä, J., Kelle, O., Lehikoinen, M., Inkinen, M., 2001. A segmentation-based method to retrieve stem volume estimates from 3-D tree height models produced by laser scanners. *IEEE*

Transactions on Geoscience and Remote Sensing, 39(5), pp. 969-975.

Joerg, P.C., Weyermann, J., Morsdorf, F., Zemp, M., Schaepman, M.E., 2015. Computation of a distributed glacier surface albedo proxy using airborne laser scanning intensity data and in-situ spectro-radiometric measurements. *Remote Sensing of Environment*, 160, pp. 31-42.

Mallet, C., Bretar, F., 2009. Full-waveform topographic lidar: State-of-the-art. *ISPRS Journal of Photogrammetry and Remote Sensing*, 64(1), pp. 1-16.

Means, J.E., Acker, S.A., Harding, D.J., 1999. Use of large-footprint scanning airborne LIDAR to estimate forest stand characteristics in the Western Cascades of Oregon. *Remote Sensing of Environment*, 67(3), pp. 298-308.

Næsset, E., Bjerknes, K.O., 2001. Estimating tree heights and number of stems in young forest stands using airborne laser scanner data. *Remote Sensing of Environment*, 78(3), pp. 328-340.

Nilsson, M., 1996. Estimation of tree heights and stand volume using an airborne LIDAR system. *Remote Sensing of Environment*, 56(1), pp. 1-7.

Smith, D.E., Zuber M.T., Frey, H.V., Garvin, J., Head, J.W., Muhleman, D.O., 1998. Topography of the northern hemisphere of Mars from the Mars orbiter laser altimeter. *Science*, 279(5357), pp. 1686-1692.

Słota, M., 2015. Full-waveform data for building roof step edge localization. *ISPRS Journal of Photogrammetry and Remote Sensing*, 106, pp. 129-144.

Tian, J., Wang, L., Li, X., 2015. Sub-footprint analysis to uncover tree height variation using ICESat/GLAS. *International Journal of Applied Earth Observation and Geoinformation*, 35, pp. 284-293.

Wagner, W., Ullrich, A., Ducic, V., Melzer, T., Studnicka, N., 2006. Gaussian decomposition and calibration of a novel small-footprint full-waveform digitising airborne laser scanner. *ISPRS Journal of Photogrammetry and Remote Sensing*, 60(2), pp. 100-112.

Wang, X., Cheng, X., Gong, P., Huang, H., Li, Z., Li, X., 2011. Earth science applications of ICESat/GLAS: a review. *International Journal of Remote Sensing*, 32(23), pp. 8837-8864.

Zwally, H.J., Schutz, B., Abdalati, W., Abshire, J., Bentley, C., Brenner, A., Bufton, J., Dezio, J., Hancock, D., Harding, D., Herring, T., Minster, B., Quinn, K., Palm, S., Spinhirne, J., Thomas, R., 2002. ICESat's laser measurements of polar ice, atmosphere, ocean, and land. *Journal of Geodynamics*, 34, pp. 405-445.